

Regioselective Fluorination of Acenes: Tailoring of Molecular Electronic Levels and Solid-State Properties

Daniel Bischof,^[a] Matthias W. Tripp,^[b] Philipp E. Hofmann,^[b] Chun-Ho Ip,^[b] Sergei I. Ivlev,^[b] Marina Gerhard,^[a] Ulrich Koert,^{*[b]} and Gregor Witte^{*[a]}

Abstract: Optoelectronic properties of molecular solids are important for organic electronic devices and are largely determined by the adopted molecular packing motifs. In this study, we analyzed such structure-property relationships for the partially regioselective fluorinated tetracenes 1,2,12-trifluorotetracene, 1,2,10,12-tetrafluorotetracene and 1,2,9,10,11-pentafluorotetracene that were further compared with tetracene and perfluoro-tetracene. Quantum chemical DFT calculations in combination with optical absorption

spectroscopy data show that the frontier orbital energies are lowered with the degree of fluorination, while their optical gap is barely affected. However, the crystal structure changes from a herringbone packing motif of tetracene towards a planar stacking motif of the fluorinated tetracene derivatives, which is accompanied by the formation of excimers and leads to strongly red-shifted photoluminescence with larger lifetimes.

Introduction


Organic electronics is an emerging field of technology that promises the fabrication of flexible and cost-effective optoelectronic devices and sensors.^[1] Although first organic devices are already available on the market,^[2] the microscopic understanding of the underlying optoelectronic processes is still incomplete, which expresses the need for further investigations and the exploration of new organic materials. Nowadays the electronic properties of single molecules can be versatily tailored through chemical design and also calculated precisely.^[3] However, the optoelectronic properties of molecular solids such as excitonic states and their dynamics, which are more relevant for device applications, are hardly predictable. This is because the latter depend on one hand critically on the molecular packing motifs in the solid,^[4] which are difficult to predict for van der Waals bound molecular solids, and on the other hand require a complex theoretical description (e.g. using *ab initio* methods and solving the Bethe-Salpeter equations)^[5]


even with knowledge of their crystal structure. In addition, planar molecular packing motifs also enable the formation of excimers,^[6] which has a decisive influence on the luminescence of such molecular solids. Therefore, well-defined model systems whose crystal structure and optoelectronic properties are known can help to enhance the understanding of this structure-property relationship.

Among the organic semiconductors, the larger acenes (pentacene and tetracene) often serve as prototypical molecular materials, as they form well-ordered crystalline films that show sufficient thermal stability and reasonably high charge carrier mobility, while their simple structure enables conceptual theoretical analyzes within the framework of Hückel theory as well as more refined density functional theory (DFT).^[7] Moreover, their aromatic frame enables versatile control of the molecular electronic structure by chemical functionalization as demonstrated in previous works.^[8] Halogenation, especially direct fluorination, is a common strategy to alter the electronic properties of organic semiconductors since the polar C–F bonds directly lower the energy levels of the π -system and change the charge density distribution within the aromatic system leading to electron accumulation at the fluorine atoms and in case of perfluorination causes an inversion of molecular quadrupole moments.^[9] Notably, the fluorination of acenes does not change the shape of the molecules but its molecular charge distribution,^[10] so that the molecular packing motif is essentially controlled by electrostatic interactions, while larger side-groups affect the molecular packing in a more complex way, as they introduce additional steric interactions.^[8d] While the perfluorination of acenes is well established,^[11] so far, only a small number of partially fluoro-substituted pentacenes and tetracenes have been synthesized, mainly with symmetrical fluorination,^[12] or in case of asymmetric substitution only at the short molecular side.^[13] Recently, a new synthetic strategy was introduced that allows a regioselective functionalization, as demonstrated by

[a] D. Bischof, Prof. Dr. M. Gerhard, Prof. Dr. G. Witte
Fachbereich Physik
Philipps-Universität Marburg
Renthof 7, 35032 Marburg (Germany)
E-mail: gregor.witte@physik.uni-marburg.de

[b] Dr. M. W. Tripp, Dr. P. E. Hofmann, C.-H. Ip, Dr. S. I. Ivlev, Prof. Dr. U. Koert
Fachbereich Chemie
Philipps-Universität Marburg
Hans-Meerwein-Straße 4, 35043 Marburg (Germany)
E-mail: koert@chemie.uni-marburg.de

 Supporting information for this article is available on the WWW under <https://doi.org/10.1002/chem.202103653>

 © 2021 The Authors. Chemistry - A European Journal published by Wiley-VCH GmbH. This is an open access article under the terms of the Creative Commons Attribution Non-Commercial License, which permits use, distribution and reproduction in any medium, provided the original work is properly cited and is not used for commercial purposes.

the example of unilaterally fluorinated pentacene and tetracene derivatives.^[14]

In this study, we expanded this strategy and synthesized various unilaterally fluorinated acenes with different degrees of fluorination. Since pentacene has a rather poor solubility, which impedes the synthesis and handling of the compounds,^[8b] we have considered tetracene derivatives here. In addition, compared to pentacene, the tetracene derivatives show pronounced fluorescence even at room temperature, which enables additional characterization through their photoluminescence (PL) properties and thereby allows to gain insights into excitonic and excimeric states.^[15] Specifically, we synthesized the partially fluorinated tetracenes 1,2,12-trifluorotetracene (F_3 TET), 1,2,10,12-tetrafluorotetracene (F_4 TET) and 1,2,9,10,11-penta-fluorotetracene (F_5 TET, synthesized as shown in Ref. [14]), determined their crystal structure and analyzed the optical absorption and PL spectra for solutions and the solid phase and compared with the corresponding properties of non-fluorinated tetracene (TET) and the perfluorinated tetracene (PFTET). Since the respective syntheses are quite laborious, we also investigated the electronic single molecule properties of other partially fluorinated tetracenes at the DFT level in order to examine this class of molecules more systematically. The identified molecular packing motifs in the crystal structures of the newly synthesized compounds are further rationalized in the frame of a Hirshfeld analysis. Interestingly, the solid state PL spectra of the partially fluorinated tetracenes reveal a distinctly red-shifted and broad signal compared to the solution spectra as well as the solid phase of the non-fluorinated tetracene, which indicates an excimeric excitation. Complementary time-resolved PL measurements also reveal distinctly longer lifetimes of the excimeric than for the excitonic states. The corresponding crystal structure analyses reveal that all fluorinated

tetracenes exhibit a (slip) stacked packing of the molecular planes while the non-fluorinated tetracene reveals a herring-bone packing, hence indicating that the latter motif hampers an excimer formation in the solid phase.

Results and Discussion

Design of unilaterally fluorinated tetracenes

When exploring a novel class of molecules, theoretical modeling is a good starting point, as it enables an *in silico* screening of the single molecular electronic properties at low cost, even for species whose synthesis could be quite challenging. Figure 1 summarizes the DFT-calculated frontier orbitals and molecular electrostatic potentials (MEPs) of partially fluorinated tetracenes with different degree of fluorination. The visualization of the frontier orbitals which have π -character shows nicely that in contrast to hydrogen atoms the fluorine atoms contribute to the π -system,^[16] but exhibit an additional nodal plane between them and the carbon atoms of the tetracene backbone. Due to their high electronegativity, fluorine atoms exhibit a strong electron-withdrawing character, which affects the charge density distribution within the molecule. In case of tetracene, a high electrostatic potential (indicated by blue color) and thus low electron density is present at the molecular rim, while a low electrostatic potential (red color) and hence a high electron density occurs in the center. In contrast, for the fluorinated species high electron density is observed at the fluorine atoms due to the polar F–C bonds and hence a lower electron density occurs in the center. For asymmetrically fluorinated tetracenes, this polarity even leads to a permanent molecular dipole moment, as visualized by grey arrows in Figure 1, while the

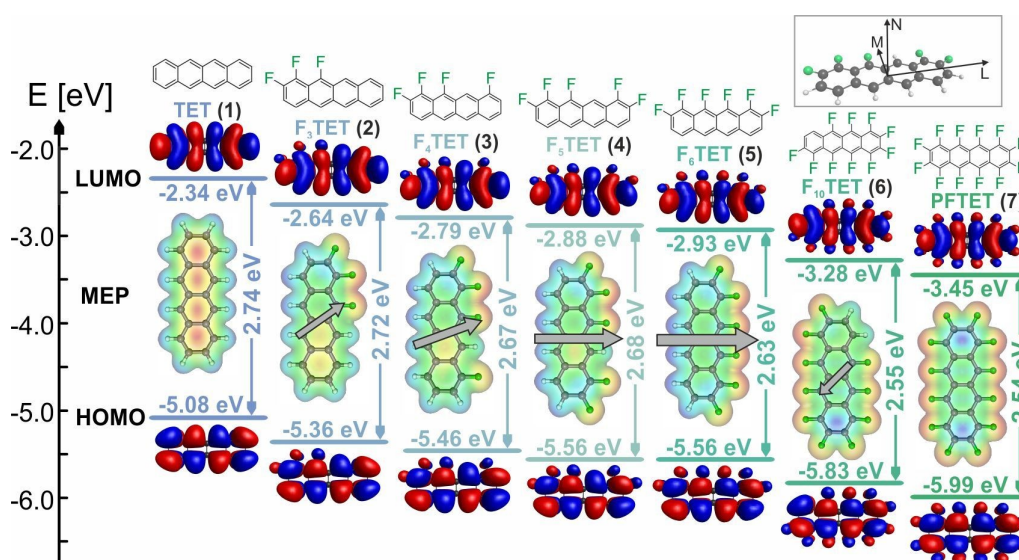


Figure 1. Comparison of electronic properties (energy levels, frontier orbitals (HOMO and LUMO) and molecular electrostatic potentials (MEPs)) of tetracene (TET; 1), trifluorotetracene (F_3 TET, 2), tetrafluorotetracene (F_4 TET, 3), pentafluorotetracene (F_5 TET, 4), hexafluorotetracene (F_6 TET, 5), decafluorotetracene (F_{10} TET, 6) and perfluorotetracene (PFTET, 7)^[11c] obtained by DFT at the B3LYP/aug-cc-pVTZ level, demonstrating that by addition of single fluorine atoms the energy levels of both frontier orbitals can be reduced by approximately 0.1 eV. Permanent dipole moments \mathbf{p} , are visualized as grey arrows.

Table 1. Comparison of the electrostatic properties (Dipole moments μ , Quadrupole moments Θ and polarizabilities α) of partially fluorinated tetracenes, given along the long axis L, the short axis M and the axis perpendicular to the molecular plane N. The values for the quadrupole moments are presented for the diagonalized tensors with the coordinate system rotated for γ degrees as shown in the Supporting Information. The dipole moments are calculated at the B3LYP/aug-cc-pVTZ level, whereas the quadrupole moments and the polarizabilities are calculated at the B3LYP/6-311G(d,p) level to ensure comparability with the literature.^[10]

Compound	μ_L [D]	μ_M [D]	μ_N [D]	$ \mu $ [D]	Θ_{xx} [10 ⁻³⁵ C cm ²]	Θ_{yy} [10 ⁻³⁵ C cm ²]	Θ_{zz} [10 ⁻³⁵ C cm ²]	γ [Deg.]	α_L [10 ⁻²⁴ cm ³]	α_M [10 ⁻²⁴ cm ³]	α_N [10 ⁻²⁴ cm ³]
TET	0	0	0	0	3.9	3.3	-7.2	0	63.7	29.6	10.7
F ₃ TET	2.41	3.38	0	4.15	-2.5	7.0	-4.4	48	63.8	29.7	10.7
F ₄ TET	1.76	4.70	0	5.02	-0.6	4.2	-3.6	55	63.6	29.8	10.7
F ₅ TET	0.24	5.56	0	5.57	-2.4	3.7	-1.3	5	64.0	29.7	10.8
F ₆ TET	0	6.56	0	6.56	-1.8	2.9	-1.1	0	64.3	30.2	10.8
F ₁₀ TET	1.98	2.06	0	2.86	4.6	-8.7	4.0	57	65.5	30.7	10.8
PFTET	0	0	0	0	-2.8	-4.6	7.5	0	66.2	30.9	10.9

numerical values are provided in Table 1. Additionally, the asymmetrically modified charge distribution also changes the molecular quadrupole moments, leading to a non-diagonal quadrupole tensor, whose main in-plane axes x and y no longer coincide with the molecular L and M axes but are rotated by the angle γ (details of the calculations are given in the Supporting Information). The obtained components of the quadrupole tensors are presented in Table 1 and show that asymmetrically fluorinated acenes have smaller quadrupole moments, as they already exhibit strong dipole moments. Interestingly, on the other hand, the degree of fluorination hardly changes the molecular polarizability (c.f. Table 1), which was also observed for pentacenes.^[14]

The electron withdrawing effect of the fluorine atoms induces a reduction of the electron density at the carbon atoms, which not only affects the electrostatic potential through the frontier orbitals, but also increases the C1s binding energy upon fluorination,^[16] which leads within the Hückel theory to a larger Coulomb integral.^[17] As tetracene is an alternant hydrocarbon, the π -orbitals occur in pairs according to the Coulson-Rushbrooke theorem^[18] so that the partial fluorination leads to a similar reduction of both frontier orbitals. This physico-chemical effect has also been observed before for other (partially) fluorinated alternant hydrocarbons such as for example hexabenzocoronenes, pentacenes or rubrenes, for which an energetic reduction of both frontier orbitals upon fluorination was also observed.^[12c,19] More precisely, our DFT calculations show that by increasing the degree of partial fluorination the frontier orbital energy levels of the tetracenes can be adjusted roughly in 0.1 eV steps per fluorine atom, while the HOMO-LUMO gap, is changed only slightly (c.f. Figure 1). Such synthetically adjustable energy levels are particularly useful for tailoring electronic properties (e.g. for tuning the work function at metal-organic interfaces).^[20] A crucial requirement for such delicate compounds, however, is their chemical synthesis. To demonstrate the influence of unilateral fluorination of tetracenes, the syntheses are realized for compounds 2 and 3, while the syntheses of 1, 4 and 7 are already known from the literature.^[11,14]

Synthesis of unilaterally fluorinated tetracenes 2 and 3

The synthesis of unilaterally fluorinated tetracenes 2 and 3 requires a synthetic approach, which allows to control the regioselectivity of the unilateral substitution patterns. Common synthetic methods based on symmetric cycloadditions do not fulfil these requirements, hence we utilize a recently developed approach with two bonds being formed in subsequent steps.^[14] In all partially fluorinated tetracene syntheses pinacolboronic ester 8^[14] was used as one coupling partner in Suzuki-couplings with different benzyl bromides which differ in their fluorine content (Figure 2).

Starting point of the synthesis for F₄TET 3 (Scheme 1) was 3-fluoro-2-hydroxybenzaldehyde (9) which was MOM-protected, reduced and subjected to Appel reaction to give the corresponding benzyl bromide 10. Suzuki-coupling^[14] with pinacolboronic ester 8 and subsequent removal of the MOM-protection group with TFA gave benzylnaphthalene 11. The phenol was triflated and the ester moiety was reduced with DIBAL and reoxidized to the corresponding aldehyde under Swern-conditions. Closure of the last ring was achieved using Ni(cod)₂ which triggers an intramolecular Barbier-type attack of the triflate on the aldehyde, yielding dihydrotetracenol 12.^[14,21] Installation of a leaving group by addition of MsCl and subsequent elimination afforded the desired F₄TET 3 (Scheme 1).

The synthesis of F₃TET 2 started from salicylic acid (13) which was esterified and MOM-protected (Scheme 2). Reduction of the ester with LiAlH₄ followed by an Appel reaction gave benzyl bromide 14.^[22] Suzuki-coupling with pinacolboronic ester 8 and MOM-deprotection using HCl obtained benzylnaphthalene 15. Following the same four-step procedure as for F₄TET, the corresponding dihydrotetracenol 16 could be isolated. The

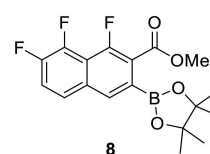
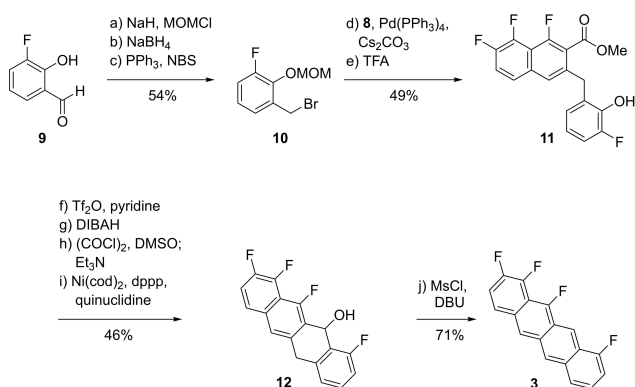
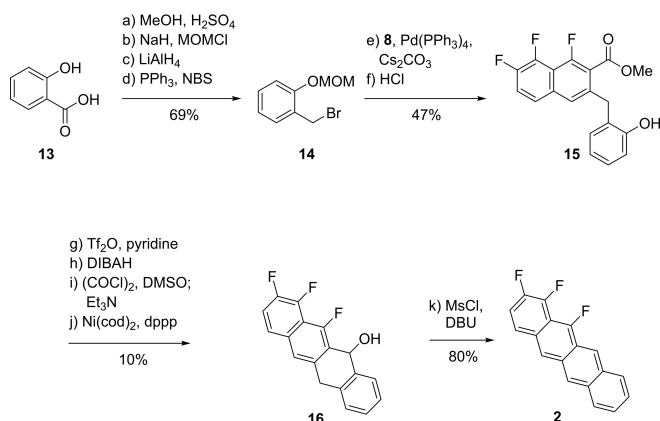


Figure 2. Common precursor for the synthesis of unilaterally substituted tetracenes.



Scheme 1. Syntheses of F_4 TET **3** using the regioselective stepwise coupling approach to build up one aromatic ring: a) NaH (1.2 eq), DMF, 0 °C, 30 min; MOMCl (1.3 eq), 0 °C, 1.5 h; b) NaBH₄ (4.0 eq), THF, r.t., 1 h; c) PPh₃ (2.0 eq), NBS (2.0 eq), CH₂Cl₂, 2 h 20 min; d) **8** (1.1 eq), Pd(PPh₃)₄ (3.0 mol%), Cs₂CO₃ (3.0 eq), THF/H₂O 10:1, 75 °C, 21 h; e) TFA (5.0 eq), CH₂Cl₂, 0 °C to r.t., 22 h; f) Tf₂O (1.2 eq), pyridine (2.8 eq), CH₂Cl₂, 0 °C, 30 min; g) DIBAH (2.5 eq), THF, 0 °C to r.t., 18 h; h) (COCl)₂ (1.5 eq), DMSO (3.0 eq), CH₂Cl₂, -78 °C, 30 min; Et₃N (5.0 eq), -78 °C, 30 min; r.t., 1 h; i) Ni(cod)₂ (1.0 eq), dppp (1.2 eq), quinuclidine (1.0 eq), toluene, 70 °C, 43 h; j) MsCl (3.0 eq), DBU (5.0 eq), CH₂Cl₂, 0 °C to r.t., 1 h; 40 °C, 2 h.



Scheme 2. Synthesis of F_3 TET **2** using the regioselective stepwise coupling approach: a) MeOH (3.0 eq), H₂SO₄ (0.3 eq), (CH₂Cl)₂, 85 °C, 23 h; b) NaH (1.5 eq), DMF, 0 °C, 30 min; MOMCl (1.5 eq), 0 °C to r.t., 45 min; c) LiAlH₄ (1.1 eq), Et₃O, 0 °C to r.t., 20 min; d) PPh₃ (2.0 eq), NBS (2.0 eq), CH₂Cl₂, 0 °C, 30 min; e) **8** (1.1 eq), Pd(PPh₃)₄ (3.0 mol%), Cs₂CO₃ (3.0 eq), THF/H₂O 10:1, 75 °C, 21 h; f) HCl, MeOH, 65 °C, 3 h; g) Tf₂O (1.2 eq), pyridine (2.8 eq), CH₂Cl₂, 0 °C, 1 h; h) DIBAH (5.5 eq), THF, 0 °C to r.t., 6 h; i) (COCl)₂ (1.5 eq), DMSO (3.0 eq), CH₂Cl₂, -78 °C, 30 min; Et₃N (5.0 eq), -78 °C, 30 min; r.t., 15 min; j) Ni(cod)₂ (1.0 eq), dppp (1.2 eq), toluene, 70 °C, 3 d; k) MsCl (3.0 eq), DBU (5.0 eq), CH₂Cl₂, 0 °C to r.t., 1 h; 40 °C, 2 h.

yield for the nickel-mediated ring-closure (14%) dropped strongly compared to the tetrafluoro-compound **12** (63%), which might be due to electronic effects of the fluorine-substituent. However, mesylation and elimination gave F_3 TET **2** in good yield (Scheme 2).

Structure analyses of unilaterally fluorinated tetracenes

With the newly synthesized compounds at hands, the next step was to identify the crystal structures in order to correlate the molecular packing motif and the optoelectronic properties of the solids. However, our previous study has shown that unilaterally fluorinated acenes crystallize poorly and only form rather small crystals.^[14] On the other hand it was found that small crystallites precipitate as powder in the last step of the synthesis of components **2–4**. Therefore, we measured and analyzed at first the corresponding powder diffractograms of the various tetracenes that are compared in Figure 3. Already from simple qualitative considerations it can be concluded that the powder patterns and thus the packing motifs of F_4 TET and F_5 TET are similar and are distinctly different to that of the non-fluorinated TET. The latter compound exhibits the two closely spaced ($1\bar{1}0$) and (112) reflections at 19.33° and 19.45°, while similar reflections are not observed for any of the (partially) fluorinated tetracenes. In such planes the TET molecules are oriented with their L-axes parallel to the plane and adopt a herringbone packing motif.^[23]

In contrast, the powder pattern of F_3 TET shows severe differences to both TET and the higher fluorinated tetracenes, which indicates the presence of a different crystal structure. In case of F_5 TET the Rietveld refinement of the powder pattern allows the determination of the crystal structure (see Supporting Information and Figure 4a), which agrees well with the previously reported structure determined by a single crystal analysis.^[14] Also for F_4 TET a Rietveld refinement was possible, yielding an isotopic crystal structure with a criss-cross packing motif. Utilizing sophisticated liquid-assisted growth techniques involving ionic liquids^[24] we have been able to grow mesoscopic single crystals of F_4 TET of a size of 50 μm x 200 μm with a thickness of several microns well suitable for single crystal

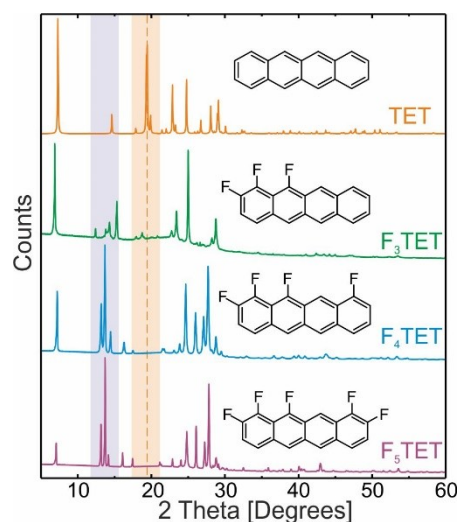


Figure 3. Powder diffractograms of F_3 TET, F_4 TET and F_5 TET measured at room temperature using Cu-K α radiation that are compared with the calculated powder spectrum of TET.^[23] The high similarities of the diffractograms for F_4 TET and F_5 TET are highlighted and are in contrast to the diffractogram of TET, revealing the presence of different crystal structures.

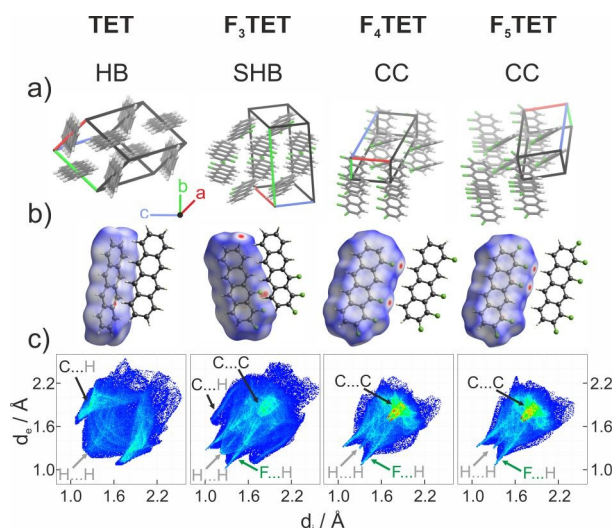


Figure 4. Comparison of a) crystal structures, b) Hirshfeld surfaces as well as c) Hirshfeld fingerprint plots (more details see Supporting Information) of the tetracene bulk structure,^[23] a proposed structure for F₃TET and the determined structures of F₄TET and F₅TET,^[14] showing characteristic molecular packing motifs: HB herringbone, SHB sandwich herringbone, CC criss-cross.

analysis by X-ray diffraction (for details see the Supporting Information). The resulting crystal structure agrees well with the one obtained by refinement of the powder measurements and is shown in Figure 4. As observed for F₅TET, also the F₄TET molecules are packed in such a way that their M-axis oriented dipole moments (cf. Figure 1) are arranged in parallel. Although this prevents a compensation of the molecular dipole moments in the crystal, it enables an additional lateral electrostatic stabilization between neighboring molecules. Interestingly, however, one finds a compensation for the non-vanishing L-axis component of the molecular dipole moment for F₄TET as the molecules are statistically flipped around the M-axis in the bulk crystal (more details see Supporting Information). While a perfect cofacial π -stacking of acenes as well as (partially) fluorinated acenes is repulsive, the F₄TET and F₅TET molecules are slip-stacked with vertical distance of their aromatic planes of about 3.4 Å, a value that is also found in the bulk structures of perfluorinated acenes.^[11] This value is somewhat larger than the closed stacking that was found for partially fluorinated hexabenzocoronone as well as the substrate stabilized π -stacked phase of perfluoropentacene or PFTET formed in films grown on graphite or graphene.^[11c,19c,25]

We note that the Rietveld refinements of F₄TET and F₅TET against the powder diffraction data revealed no impurity peaks indicating the phase purity of the synthesized materials. Moreover, as the powder and single crystal measurements were carried out at different temperatures (RT vs. 100 K), the anisotropic thermal expansion of these compounds could also be determined and revealed a larger thermal expansion along the b-axis than for the a- and c-axes (for more details see Supporting Information).

Although mesoscopic crystals could also be grown for F₃TET using liquid-assisted growth, these were not stable during the X-ray analysis, which indicates possible radiation damage. The higher solubility of F₃TET also enabled the growth of single crystals from toluene solution by evaporation of the solvent. While the resulting red crystals are suitable for optical spectroscopy and exhibit slightly different optical properties than the powder (for more details see Supporting Information), they were too small for crystal structure analysis. Hence, we tried to determine the crystal structure of F₃TET by powder diffractometry. Unfortunately, however, the powder pattern did not allow an unambiguous determination of the structure. Therefore, we have compared the possible unit cells to identify the most plausible structure (see Supporting Information). Comparing the density accompanied with the different unit cells and using geometrical considerations (see Supporting Information), the most plausible crystal structure, which is consistent with the powder pattern, exhibits a sandwich-herringbone motif with pairs of molecules tilted in the same direction arranged in a herringbone pattern as depicted in Figure 4a. We note that a similar packing motif has been reported for electronically similar 5-halogenated tetracenes,^[26] hence supporting our hypothesis. Moreover, the presence of molecular sandwich pairs is further corroborated by our PL measurements of F₃TET solid as discussed in the next section.

To rationalize the intermolecular interactions leading to such different packing motifs, we have performed a Hirshfeld analysis and present the Hirshfeld surfaces as well as the 2D-fingerprint plots in Figure 4b and c (for details on Hirshfeld analysis, see refs 27). Here we concentrate first on the presence of F...H interactions, as observed for partially fluorinated tetracenes. These interactions are indicated as red contact points on the Hirshfeld surface (cf. Figure 4b) and are visible in the 2D fingerprint plots as characteristic wings (indicated by green arrows in Figure 4d). Due to their high frequency (more than 30%/40%/45% of all contact points for F₃TET/F₄TET/F₅TET) they favor the formation of non-herringbone packing motifs. Additionally, there are pronounced C...C interactions visible in the fingerprint plots of F₄TET and F₅TET, which resemble a slip stacked packing along the crystallographic b-axis. Also, for the proposed sandwich herringbone packing of F₃TET the reminiscence of slip stacked packing is observed, while such interactions are absent in the fingerprint plots of tetracene, where molecules adopt a face-on-edge herringbone packing motif. Our analysis thus shows that the introduction of fluorine atoms can drastically change the molecular packing in the solids of the tetracene derivatives, since it modifies the balance of intermolecular interactions as observed before also for other partially fluorinated molecules.^[28]

Optical properties of unilaterally fluorinated tetracenes

Next, we investigate the optoelectronic properties of the tetracenes in solution and solid state. Since the here presented synthetic route yields phase pure powders, we used them for solid state spectroscopy to exclude anisotropic absorption due

to preferential molecular orientations in the crystals.^[29] For tetracene, however, impurities appeared in the powder spec-

trum of the raw material, which is why we recorded the optical spectra on single-crystals as described in the Supporting Information. The results are further compared with optical properties of PFTET crystals of the α -phase studied previously.^[11c]

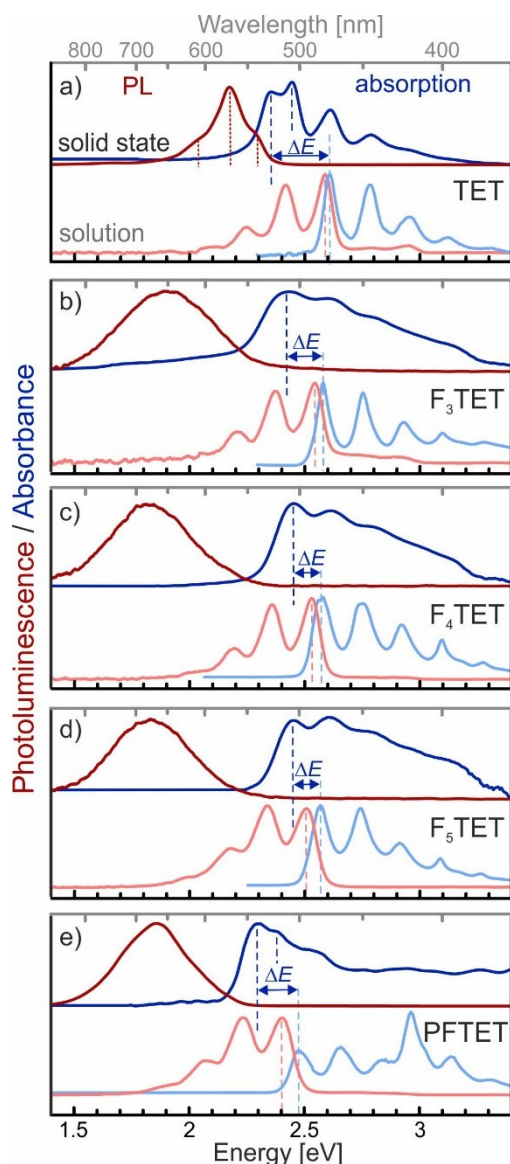


Figure 5. Comparison of the absorbance of the investigated tetracenes (a) TET, b) F₃TET, c) F₄TET, d) F₅TET and e) PFTET^[11c] in CH₂Cl₂ solution (bright blue) and solid films (dark blue) with labelled maximum of lowest absorption bands E_G and the energy differences $\Delta E = E_G^{\text{solu}} - E_G^{\text{solid}}$ as well as the photoluminescence in toluene solution (bright red) and solid state (dark red).

Figure 5 summarizes the UV/Vis absorption and PL spectra of the differently fluorinated tetracenes in solution (bright color spectra, in lower row of each panel) and the solid phase (dark color spectra, upper rows), which are further compared with corresponding data of TET and PFTET. The solution spectra nicely reveal the complementarity of UV/Vis and PL spectroscopy and exhibit only small Stokes shifts confirming that the low energy absorption band is caused by the 0-0 transition and gives the HOMO-LUMO gap E_G^{solu} followed by vibronic progressions. Since the energy of both frontier orbitals (HOMO, LUMO) decreases with increasing degree of fluorination, as listed in Table 2, E_G^{solu} only changes slightly upon partial fluorination. This is in close agreement with the calculated values, rendering fluorination a feasible tool to engineer frontier orbital energies almost without affecting the HOMO-LUMO gap. Interestingly, with higher degree of fluorination the highest energetic emission $E_{\text{em}}^{\text{solu}}$ decreases slightly more than E_G^{solu} causing an increased Stokes shift. Notably the solution absorption spectrum of PFTET reveals an additional distinct absorption band at 2.95 eV (cf. Figure 5e), which was identified as the HOMO-LUMO+1 transition,^[11c] while corresponding transitions of non- or partially-fluorinated tetracenes occur at higher energies that are outside the probed energy region.

By contrast the optical solid state spectra reveal distinct differences. For each molecular solid the absorption spectra reveal a lower energetic absorption band than for the solutions due to excitations of excitonic states^[31] and in case of TET and PFTET even exhibits a fine structure due to the Davydov components of the singlet excitons.^[32] A precise determination of the exciton binding energy, which in the Frenkel picture is defined as the energy difference between a bound electron-hole pair and the fundamental gap (i.e. the difference between the ionization potential (IP) and the electron affinity (EA) of an isolated molecule), requires knowledge of the latter values and is not so easy. In the solid-state picture an exciton describes a quasiparticle, whose binding energy is given by the difference of the optical gap and the transport gap,^[31] where the transport gap is typically determined by combining photoelectron and inverse photo-emission spectroscopy. As these values could not be determined in this study either, we instead consider the

Table 2. Comparison of optoelectronic properties of partially fluorinated tetracenes: Calculated energy levels (B3LYP/aug-cc-pVTZ) and the corresponding optical gap, experimentally determined optical gap from UV/Vis absorption spectroscopy for solution and solid films (i.e. exciton), the energy difference $\Delta E = E_G^{\text{solu}} - E_G^{\text{solid}}$, the highest energetic emission in solution and the energy difference of the Stokes shift $\Delta E_{\text{Stokes}} = E_G^{\text{solu}} - E_{\text{em}}^{\text{solu}}$. All energies are given in eV.

Compound	HOMO ^{DFT}	LUMO ^{DFT}	E_G^{DFT}	E_G^{solu}	E_G^{solid}	ΔE	$E_{\text{em}}^{\text{solu}}$	ΔE_{Stokes}
TET ^[a]	-5.08	-2.34	2.74	2.61	2.36	0.25	2.59	0.02
F ₃ TET	-5.36	-2.64	2.72	2.58	2.43	0.15	2.55	0.03
F ₄ TET	-5.46	-2.79	2.67	2.57	2.45	0.12	2.53	0.04
F ₅ TET	-5.56	-2.88	2.68	2.57	2.45	0.12	2.51	0.06
PFTET ^[a]	-5.99	-3.45	2.54	2.48	2.30	0.18	2.40	0.08

[a] Data taken from Ref. [11c].

energy difference between the optical excitation of molecules in solution and in the solid $\Delta E = E_G^{\text{solu}} - E_G^{\text{solid}}$ as a measure of the influence of the dielectric screening of the molecular solid on the excitonic excitation. Interestingly, for fluorinated tetracenes this quantity, which is related to the exciton binding energy, is substantially smaller than for unsubstituted tetracene. A similar trend has also been observed for other perfluorinated acenes.^[11c] This difference can be explained by the different molecular packing motifs herringbone vs. planar stacking, which are found also in a previous study on substituted pentacenes to affect the exciton binding.^[8d]

Remarkably, the solid state PL spectra of all studied fluorinated tetracenes have one characteristic in common, namely a red-shifted broad emission, which does not occur in the solution PL spectra of all tetracene derivatives or in the solid state PL spectrum of the normal TET. Similar features have been observed before in PL spectra for saturated solutions of pyrene or perylene^[33] and later also for some organic solids^[34] and were attributed to excimeric excitations.

To further characterize these excitations, we performed time-resolved photoluminescence (TR-PL) measurements of fluorinated tetracenes in solution and in the solid state. While the transient PL of tetracene and fluorinated tetracenes in solution is very similar (see Supporting Information) and thus indicates comparable relaxation dynamics, a more diverse situation is observed in the solid state, as depicted in Figure 6. Here, the PL decay of TET and F₃TET is remarkably faster than the decay in F₄TET and F₅TET. The times, after which the PL transients of TET and F₃TET have decayed to a fraction of 1/e of their initial intensity are 0.7 ns and 1 ns, respectively. For the longer-lasting signals of F₄TET and F₅TET, the time window provided by our instrumentation was not suitable for an accurate determination of the PL lifetimes. However, an estimation of the intensity ratio between the signal maximum at $t=0$ and the residual PL signal from the previous laser pulse at $t < 0$ yields PL lifetimes of the F₄TET and the F₅TET signatures on the order of 4–5 ns.

These severe changes in lifetimes arise either from the different molecular packing in the solids or from the individual

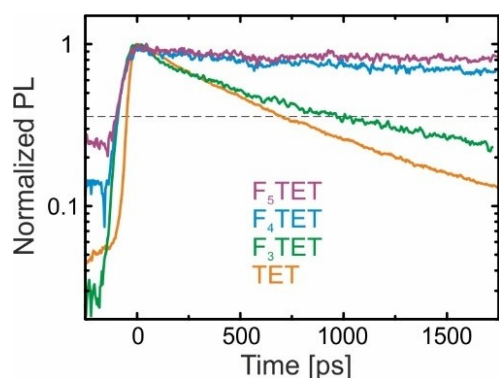


Figure 6. Normalized time-resolved photoluminescence transients of unilaterally fluorinated tetracenes in solid state ($\lambda_{\text{excitation}} = 435$ nm, measured at 78 K). The dashed line serves as guide to the eye, to indicate at which time the transients have decayed to a fraction of 1/e of their initial amplitude.

single molecule properties. Since the PL signatures and transients in solution are very similar for all partially and non-fluorinated tetracenes, the second possibility can be ruled out, suggesting that the emission properties are mainly determined by the molecular packing. Indeed, the differences in the decay dynamics coincide with the underlying packing motifs. Tetracene with a sub-ns excitonic emission crystallizes in the herringbone structure. On the other hand, F₄TET and F₅TET with significantly longer decay dynamics in the solid state exhibit a criss-cross packing motif with planar stacking of molecules due to changed electrostatic interactions. The sandwich herringbone motif of F₃TET can be considered as an intermediate between the two former cases, combining face-on-edge packing with planar stacking. As planar stacking of the molecules is an important prerequisite for excimer formation, we thus conclude that the longer decay and the red-shifted, broad and structureless emission in the fluorinated tetracenes is related to excimers. This is further supported by PL studies of purely disordered solid tetracene, where long-lived excimeric emission was reported at similar emission energies.^[35] In contrast to these longer lived species, (poly-)crystalline tetracene shows a faster decay because of efficient singlet fission.^[15b-d] Note that also for polycrystalline tetracene certain bands between 570 nm and 700 nm were reported and assigned to defect states,^[36] but in some other cases they were also attributed to excimer emission arising from planar packing at defects. The latter assignment is, however, not consistent with the intermolecular interactions between acenes,^[10] which precludes a coplanar stacking of tetracene due to repulsive interactions between the molecular π -systems. This nicely demonstrates that the systematic study of the structure-property interrelations of fluorinated tetracenes allows to draw general conclusions, in this case about the solid state emission of unsubstituted tetracene.

At this point it should be noted that a lower fluorescence of molecules is often observed in the aggregated solid than in solution, which is referred to as aggregation-caused quenching (ACQ) typically based on intensity analyses, but less frequently taking spectral or life time changes into account.^[37] Since all (partially) fluorinated acenes investigated here are planar and rigid without flexible side groups, conformational changes can be completely excluded, so that the observed differences in luminescence can be attributed to the different packing motifs and couplings in the solid. Specifically, we attribute our observations to a competition between direct exciton emission and the non-radiative singlet fission or an excimer formation and emission. In order to be able to assess the influence of these individual contributions more precisely, further time-resolved measurements are necessary.

Conclusion

In this study, we have demonstrated the feasibility of regioselective functionalization of tetracenes by syntheses of the partially fluorinated tetracenes 1,2,12-trifluorotetracene and 1,2,10,12-tetrafluorotetracene. By comparing the electronic

structure of these molecules with tetracene, perfluorotetracene and the previously synthesized 1,2,9,10,11-pentafluorotetracene, we found that the degree of partial fluorination can be a synthetic tool to chemically engineer the energies of the frontier orbitals, without changing the optical HOMO-LUMO gap, obtained in solution spectra.

Interestingly, partial fluorination not only changes the energy levels, but also results in a different packing motif in the molecular solid with planarly stacked molecules instead of face-on-edge herringbone packing as observed for the non-fluorinated tetracene. Such a planar stacking enables the formation of excimers upon photoexcitation of the partially fluorinated tetracene solids, as evidenced by a red-shifted and broad band fluorescence when compared to the unsubstituted tetracene.

More generally, our results emphasize that single molecule characterization is not sufficient, but instead the solid-state properties have to be taken into account when designing and validating new molecular materials for application in organic electronics, as the molecular packing may lead to the formation of excimeric states, which can dominate the emission of molecular solids. Since the crystal structures of the fluorinated acenes investigated here are known, this enables a precise structure-property correlation and the investigation of the influence of molecular packing motifs on the optical properties. This can serve as a model system for future theoretical investigations of excimers.

Experimental Section

Experimental conditions and detailed experimental procedures for Schemes 1–2, as well as ^1H , ^{13}C and ^{19}F NMR spectra and X-ray data, as well as details on quantum chemical calculations, sample preparation, X-ray diffraction, Hirshfeld analysis and optical spectroscopy are provided in the Supporting Information.

Deposition Number 2114488 (for **3**) contains the supplementary crystallographic data for this paper. These data are provided free of charge by the joint Cambridge Crystallographic Data Centre and Fachinformationszentrum Karlsruhe Access Structures service.

Acknowledgements

The authors acknowledge support by the German Research Foundation (DFG) in the framework of the Collaborative Research Center “Structure and Dynamics of Internal Interfaces” (223848855-SFB1083, TP A2, A8 and B10). M.G. thanks Prof. Dr. Martin Koch for his support and the provided experimental equipment. Open Access funding enabled and organized by Projekt DEAL.

Conflict of Interest

The authors declare no conflict of interest.

Data Availability Statement

The data that support the findings of this study are available from the corresponding author upon reasonable request.

Keywords: acenes · electronic structure · fluorinated acenes · synthesis design · unilateral substitution

- [1] a) *Organic Electronics: Materials, Manufacturing and Applications*, (Ed.: H. Klauk), Wiley-VCH, Weinheim, **2006**; b) J.-L. Brédas, S. R. Marder in *The WSPC reference on organic electronics: Organic Semiconductors, Vols. 1 and 2*, World Scientific, Singapore, **14**, **2016**.
- [2] a) Y. S. Rim, S.-H. Bae, H. Chen, N. De Marco, *Adv. Mater.* **2016**, *28*, 4415–4440; b) H. Ling, S. Liu, Z. Zheng, F. Yan, *Small Methods* **2018**, *2*, 1800070; c) W. Tang, Y. Huang, L. Han, R. Liu, Y. Su, X. Guo, F. Yan, *J. Mater. Chem. C* **2019**, *7*, 790–808; d) Y. Bonnasieux, C. J. Brabec, Y. Cao, T. B. Carmichael, M. L. Chabiny, K.-W. Cheng, G. Cho, A. Chung, C. L. Cobb, A. Distler, H.-J. Egelhaaf, G. Grau, X. Guo, G. Haghighatiani, T.-C. Huang, M. M. Hussain, B. Iniguez, T.-M. Lee, L. Li, Y. Ma, D. Ma, M. C. Alpine, T. N. Ng, R. Österbacka, S. N. Patel, J. Peng, H. Peng, J. Rivnay, L. Shao, D. Steingart, R. A. Street, V. Subramanian, L. Torsi, Y. Wu, *Flex. Print. Electron.* **2022**, *6*, 023001.
- [3] L. Wang, N. Guangjun, X. Yang, Q. Peng, Q. Li, Z. Shuai, *Chem. Soc. Rev.* **2010**, *39*, 423–434.
- [4] K. Kolata, T. Breuer, G. Witte, S. Chatterjee, *ACS Nano* **2014**, *8*, 7377–7383.
- [5] a) C. Ambrosch-Draxl, D. Nabok, P. Puschnig, C. Meisenbichler, *New J. Phys.* **2009**, *11*, 125010; b) L. Kronik, J. B. Neaton, *Annu. Rev. Phys. Chem.* **2016**, *67*, 587–616; c) D. Golze, M. Dvorak, P. Rinke, *Front. Chem.* **2019**, *7*, 377.
- [6] a) W. T. Yip, D. H. Levy, *J. Phys. Chem.* **1996**, *100*, 11539–11545; b) H. Saigusa, E. C. Lim, *Acc. Chem. Res.* **1996**, *29*, 171–178; c) R. D. Pensack, R. J. Ashmore, A. L. Paoletta, G. D. Scholes, *J. Phys. Chem. C* **2018**, *122*, 21004–21017; d) J. Vollbrecht, *New J. Chem.* **2018**, *42*, 11249–11254.
- [7] a) E. Hückel, *Z. Phys.* **1932**, *76*, 628–648; b) J. Cornil, J. P. Calbert, J. L. Brédas, *J. Am. Chem. Soc.* **2001**, *123*, 1250–1251.
- [8] a) J. E. Anthony, J. S. Brooks, D. L. Eaton, S. R. Parkin, *J. Am. Chem. Soc.* **2001**, *123*, 9482–9483; b) J. E. Anthony, *Angew. Chem. Int. Ed.* **2008**, *47*, 452–483; *Angew. Chem.* **2008**, *120*, 460–483; c) U. H. F. Bunz, J. U. Engelhart, B. D. Lindner, M. Schaffroth, *Angew. Chem. Int. Ed.* **2013**, *52*, 3810–3821; *Angew. Chem.* **2013**, *125*, 3898–3910; d) J. Schwaben, N. Münster, M. Klues, T. Breuer, P. Hofmann, K. Harms, G. Witte, U. Koert, *Chem. Eur. J.* **2015**, *21*, 13758–13771; e) B. Shen, T. Geiger, R. Einholz, F. Reichert, S. Schundelmeier, C. Maichle-Mössmer, B. Speiser, H. F. Bettinger, *J. Org. Chem.* **2018**, *83*, 3149–3158; f) R. R. Tykwinski, *Acc. Chem. Res.* **2019**, *52*, 2056–2069; g) T. Wiesner, L. Ahrens, F. Rominger, J. Freudenberg, U. H. F. Bunz, *Chem. Eur. J.* **2021**, *27*, 4553–4556.
- [9] M. L. Tang, Z. Bao, *Chem. Mater.* **2011**, *23*, 446–455.
- [10] M. Klues, G. Witte, *CrystEngComm* **2018**, *20*, 63–74.
- [11] a) Y. Sakamoto, T. Suzuki, M. Kobayashi, Y. Gao, Y. Fukai, Y. Inoue, F. Sato, S. Tokito, *J. Am. Chem. Soc.* **2004**, *126*, 8138–8140; b) Y. Sakamoto, T. Suzuki, M. Kobayashi, Y. Gao, Y. Inoue, S. Tokito, *Mol. Cryst. Liq. Cryst.* **2006**, *444*, 225–232; c) D. Bischof, M. Zeplichal, S. Anhäuser, A. Kumar, M. Kind, F. Kramer, M. Bolte, S. I. I. Ivlev, A. Terfort, G. Witte, *J. Phys. Chem. C* **2021**, *125*, 19000–19012.
- [12] a) R. P. Bula, I. M. Opper, H. F. Bettinger, *J. Org. Chem.* **2012**, *77*, 3538–3542; b) M. W. Tripp, U. Koert, *Beilstein J. Org. Chem.* **2020**, *16*, 2136–2140; c) T. Geiger, S. Schundelmeier, T. Hummel, M. Ströbele, W. Leis, M. Seitz, C. Zeiser, L. Moretti, M. Maiuri, G. Cerullo, K. Broch, J. Vahland, K. Leo, C. Maichle-Mössmer, B. Speiser, H. F. Bettinger, *Chem. Eur. J.* **2020**, *26*, 3420–3434.
- [13] a) C.-T. Chien, T.-C. Chiang, M. Watanabe, T.-H. Chao, Y. J. Chang, Y.-D. Lin, H.-K. Lee, C.-Y. Liu, C.-H. Tu, C.-H. Sun, T. J. Chow, *Tetrahedron Lett.* **2013**, *54*, 903–906; b) C.-T. Chien, M. Watanabe, T. J. Chow, *Tetrahedron* **2015**, *71*, 1668–1673; c) C. Zeiser, L. Moretti, T. Geiger, L. Kalix, A. M. Valencia, M. Maiuri, C. Cocchi, H. F. Bettinger, G. Cerullo, K. Broch, *J. Phys. Chem. Lett.* **2021**, *12*, 7453–7458.
- [14] P. E. Hofmann, M. W. Tripp, D. Bischof, Y. Grell, A. L. C. Schiller, T. Breuer, S. I. Ivlev, G. Witte, U. Koert, *Angew. Chem. Int. Ed.* **2020**, *59*, 16501–16505; *Angew. Chem.* **2020**, *132*, 16644–16648.
- [15] a) S.-H. Lim, T. G. Bjorklund, F. C. Spano, C. J. Bardeen, *Phys. Rev. Lett.* **2004**, *92*, 107402; b) J. J. Burdett, C. J. Bardeen, *J. Am. Chem. Soc.* **2012**,

- 134, 8597–8607; c) M. J. Y. Tayebjee, R. G. C. R. Clady, T. W. Schmidt, *Phys. Chem. Chem. Phys.* **2013**, *15*, 14797–14805; d) M. W. B. Wilson, A. Rao, K. Johnson, S. Gélinas, R. di Pietro, J. Clark, R. H. Friend, *J. Am. Chem. Soc.* **2013**, *135*, 16680–16688; e) D. H. Arias, J. L. Ryerson, J. D. Cook, N. H. Damrauer, J. C. Johnson, *Chem. Sci.* **2016**, *7*, 1185–1191; f) C. B. Dover, J. K. Gallaher, L. Frazer, P. C. Tapping, A. J. Petty, M. J. Crossley, J. E. Anthony, T. W. Kee, T. W. Schmidt, *Nat. Chem.* **2018**, *10*, 305–310; g) J. Gierschner, J. Shi, B. Milián-Medina, D. Roca-Sanjuán, S. Varghese, S. Y. Park, *Adv. Opt. Mater.* **2021**, *9*, 2002251.
- [16] M. Klues, P. Jerabek, T. Breuer, M. Oehzelt, K. Hermann, R. Berger, G. Witte, *J. Phys. Chem. C* **2016**, *120*, 12693–12705.
- [17] W. E. Wentworth, L. W. Kao, R. S. Becker, *J. Phys. Chem.* **1975**, *79*, 1161–1169.
- [18] C. A. Coulson, G. S. Rushbrooke, *Math. Proc. Cambridge Philos. Soc.* **1940**, *36*, 193–200.
- [19] a) B. M. Medina, D. Beljonne, H.-J. Egelhaaf, J. Gierschner, *J. Chem. Phys.* **2007**, *126*, 11101; b) F. Anger, T. Breuer, A. Ruff, M. Klues, A. Gerlach, R. Scholz, S. Ludwigs, G. Witte, F. Schreiber, *J. Phys. Chem. C* **2016**, *120*, 5515–5522; c) T. Breuer, M. Klues, P. Liesfeld, P. Viertel, M. Conrad, S. Hecht, G. Witte, *Phys. Chem. Chem. Phys.* **2016**, *18*, 33344–33350.
- [20] A. Franco-Cañellas, S. Duhm, A. Gerlach, F. Schreiber, *Rep. Prog. Phys.* **2020**, *83*, 066501.
- [21] a) J. K. Vandavasi, X. Hua, H. B. Halima, S. G. Newman, *Angew. Chem. Int. Ed.* **2017**, *56*, 15441–15445; *Angew. Chem.* **2017**, *129*, 15643–15647; b) T. Verheyen, L. van Turnhout, J. K. Vandavasi, E. S. Isbrandt, W. M. De Borggraeve, S. G. Newman, *J. Am. Chem. Soc.* **2019**, *141*, 6869–6874.
- [22] G. A. Kraus, N. Zhang, *J. Org. Chem.* **2000**, *65*, 5644–5646.
- [23] D. Holmes, G. Kumaraswamy, A. J. Matzger, K. P. C. Vollhardt, *Chem. Eur. J.* **1999**, *5*, 3399–3412.
- [24] Y. Takeyama, S. Maruyama, Y. Matsumoto, *Cryst. Growth Des.* **2011**, *11*, 2273–2278.
- [25] I. Salzmann, A. Moser, M. Oehzelt, T. Breuer, X. Feng, Z.-Y. Juang, D. Nabok, R. G. Della Valle, S. Duhm, G. Heimel, A. Brillante, E. Venuti, I. Bilotti, C. Christodoulou, J. Frisch, P. Puschnig, C. Draxl, G. Witte, K. Müllen, N. Koch, *ACS Nano* **2012**, *6*, 10874–10883.
- [26] H. Moon, R. Zeis, E.-J. Borkent, C. Besnard, A. J. Lovinger, T. Siegrist, C. Kloc, Z. Bao, *J. Am. Chem. Soc.* **2004**, *126*, 15322–15323.
- [27] a) M. A. Spackman, D. Jayatilaka, *CrystEngComm* **2009**, *11*, 19–32; b) P. R. Spackman, M. J. Turner, J. J. McKinnon, S. K. Wolff, D. J. Grimwood, D. Jayatilaka, M. A. Spackman, *J. Appl. Crystallogr.* **2021**, *54*, 1006–1011.
- [28] K. Reichenbacher, H. I. Süß, J. Hulliger, *Chem. Soc. Rev.* **2005**, *34*, 22–30.
- [29] T. Breuer, G. Witte, *Phys. Rev. B* **2011**, *83*, 155428.
- [30] A. O. F. Jones, B. Chattopadhyay, Y. H. Geerts, R. Resel, *Adv. Funct. Mater.* **2016**, *26*, 2233–2255.
- [31] J.-L. Bredas, *Mater. Horiz.* **2014**, *1*, 17.
- [32] J. Helzel, S. Jankowski, M. El Helou, G. Witte, W. Heimbrodt, *Appl. Phys. Lett.* **2011**, *99*, 211102.
- [33] a) K. Yoshihara, T. Kasuya, A. Inoue, S. Nagakura, *Chem. Phys. Lett.* **1971**, *9*, 469–472; b) P. C. Johnson, H. W. Offen, *Chem. Phys. Lett.* **1972**, *18*, 258–260.
- [34] B. Walker, H. Port, H. C. Wolf, *Chem. Phys.* **1985**, *92*, 177–185.
- [35] G. Peter, H. Bässler, *Chem. Phys.* **1980**, *49*, 9–16.
- [36] M. Voigt, A. Langner, P. Schouwink, J. M. Lupton, R. F. Mahrt, M. Sokolowski, *J. Chem. Phys.* **2007**, *127*, 114705.
- [37] a) Y. Hong, J. W. Y. Lam, B. Z. Tang, *Chem. Soc. Rev.* **2011**, *40*, 5361–5388; b) J. Mei, N. L. C. Leung, R. T. K. Kwok, J. W. C. Lam, B. Z. Tang, *Chem. Rev.* **2015**, *115*, 11718–11940; c) Z. Zhao, H. Zhang, J. W. Y. Lam, B. Z. Tang, *Angew. Chem. Int. Ed.* **2020**, *59*, 9888–9907; *Angew. Chem.* **2020**, *132*, 9972–9993; d) F. Würthner, *Angew. Chem. Int. Ed.* **2020**, *59*, 14192–14196; *Angew. Chem.* **2020**, *132*, 14296–14301.

Manuscript received: October 8, 2021

Accepted manuscript online: December 7, 2021

Version of record online: January 3, 2022